# Storage Efficiency and Reduced Complexity Modelling

Iain de Jonge-Anderson[*1], Hariharan Ramachandran[1], Uisdean Nicholson[1], Sebastian Geiger[2], Ana Widyanita[3], Florian Doster[1]

[1]Institute of GeoEnergy Engineering (IGE), School of Energy, Geoscience, Infrastructure & Society, Heriot-Watt University, Edinburgh, EH14 4AS, UK

[2]Faculty of Civil Engineering and Geosciences, TU Delft, 2628 CN Delft, Netherlands

[3]PETRONAS Research Sdn. Bhd., Malaysia

*Corresponding author (email: i.anderson@hw.ac.uk, X: @iaindja)

ORCiD: 0000-0002-9438-8194 (IdJ-A)

**Storage Efficiency and Reduced Complexity Modelling**

Iain de Jonge-Anderson*[1], Hariharan Ramachandran[1], Uisdean Nicholson[1], Sebastian Geiger[2], Ana Widyanita[3], Florian Doster[1]

[1]Institute of GeoEnergy Engineering (IGE), School of Energy, Geoscience, Infrastructure & Society, Heriot-Watt University, Edinburgh, EH14 4AS, UK

[2]Faculty of Civil Engineering and Geosciences, TU Delft, 2628 CN Delft, Netherlands

[3]PETRONAS Research Sdn. Bhd., Malaysia

*Corresponding author (email: i.anderson@hw.ac.uk)

ORCiD: 0000-0002-9438-8194 (IdJ-A)

## Acknowledgements

The funding and data underpinning this work was provided by PETRONAS via the PETRONAS Centre of Excellence in Subsurface Engineering and Energy Transition (PACESET), based at Heriot-Watt University. Dr Raj Deo Tewari is gratefully acknowledged for providing review and constructive feedback on the manuscript. SLB is thanked for providing an academic licence for Petrel which facilitated this work.

## Abstract

Carbon capture and storage (CCS) is vital to reducing greenhouse gas emissions and mitigating climate change. Most CCS projects rely on the permanent geological storage of $CO_2$ within deep sedimentary rock formations, but accurately constraining the capacity of these reservoirs usually involves detailed and computationally demanding reservoir modelling and simulation of the pressure evolution and $CO_2$ plume migration. In the absence of this, efficiency factors are often used within volumetric capacity estimates, but this often results in overestimations of storage capacity. As an alternative, we propose a workflow harnessing various, existing, reduced complexity models that account for the surface topography and dynamic fluid behaviour in a computationally efficient manner. We first undertook a static

analysis using algorithms available within MRST-co2lab. The reservoir topography is used to determine the locations of structural traps, the trapping routes that link them and downdip filling areas that feed a given trap. This analysis provides indications of the optimal well placement and helps us refine the total capacity of the area into the capacity available just from structural trapping. We followed this with a dynamic analysis, also within MRST-co2lab, using computationally efficient Vertical Equilibrium models. This efficiency allowed us to performing hundreds of simulations and use these results to map storage efficiency and determine the optimal well placement where efficiency is greatest. We tested this workflow within an area of the Malay Basin with illustrative reservoir parameters and estimated storage efficiency, capacity and the optimal well placement within the area without performing any full-physics simulations. The results from VE modelling indicate that the amount that can be contained within this area is 15 times less than the predictions using static storage efficiency factors. The advantage of such a light approach is that sensitivity and uncertainty analysis can be carried out at speed, before targeting certain parameters/areas for more detailed study.

## Keywords

Carbon Capture and Storage (CCS), Storage capacity, Vertical Equilibrium models, Trap Analysis, Malay Basin

## 1. Introduction

The permanent storage of $CO_2$ within deep geological formations is critical to making deep greenhouse gas emissions cuts and mitigating climate change (IPCC, 2023). Evaluating the capacity of a geological storage site is key, but defining and calculating it involves various approaches and definitions. Capacity estimates during the initial stages of a project often

48 neglect the dynamic behaviour of the reservoir in favour of a volumetric approach that
49 considers just the static pore volume available for storage (Bachu et al., 2007). Efficiency
50 factors are often used to parameterise dynamic effects within the reservoir and are defined
51 as the proportion of $CO_2$ retained within the reservoir versus its pore volume considering
52 geology (permeability, connectivity, etc) and other subsurface and operational criteria
53 including pressure, injection strategy, and regulatory constraints (Bachu, 2015; Mathias et al.,
54 2015; Nordbotten & Celia, 2011). Efficiency factors are widely used within national and
55 international CO2 storage screening programmes including those in the UK (Bentham et al.,
56 2014), USA (Goodman et al., 2011) and Europe (Vangkilde-Pedersen et al., 2009).

57 Efficiency factors are helpful in constraining storage capacity at the screening level, but in the
58 absence of simulation models or long-term working injection analogues, they are selected
59 based on reservoir characteristics (e.g., environment of deposition). Storage capacity is often
60 overestimated when pressure evolution and compressibility are neglected (Thibeau & Mucha,
61 2011). Accurate calculations using full physics reservoir simulators are required to quantify
62 fluid flow through the reservoir. This usually requires a detailed knowledge of the subsurface
63 which is difficult and expensive to obtain at the early stages of the project, though recent work
64 has sought to expedite this process, for example by constructing quick, sketch-based reservoir
65 models (Jackson et al., 2022). Analytical expressions can be used to estimate flow behaviour
66 (Nordbotten et al., 2005), and in doing so, derive a quick understanding of efficiency factors
67 (Okwen et al., 2010) but they are limited in their ability to handle spatial changes in subsurface
68 geology. As a midpoint between full physics simulations and analytical expressions, Vertical
69 Equilibrium (VE) models have been successfully used to represent $CO_2$ plume behaviour
70 (Gasda et al., 2009; Nilsen et al., 2011). In typical saline aquifer conditions, there is a significant
71 density contrast between brine and $CO_2$, leading to gravity segregation. This behaviour is

exploited by assuming that upon $CO_2$ injection, pressure equilibrium is rapidly established in the vertical direction and the $CO_2$ plume height is then expressed as a function of capillary and buoyancy forces (Nordbotten & Celia, 2011). This simplification allows for the reduction of the governing equations into a lower-dimensional system, significantly reducing computational complexity.

Here we report on an improved workflow for estimating $CO_2$ storage efficiency by incorporating static and dynamic reduced complexity models. The presented approach helps calculate more realistic capacity estimates when compared with static equation-based estimates. To illustrate this approach, our workflow is deployed within small area of the Malay Basin, offshore Peninsular Malaysia ('J Area') (Figure 1). The Malay Basin is a mature hydrocarbon province that has substantial $CO_2$ storage potential. The storage capacity within saline aquifers alone is potentially 84 – 114 Gt (Hasbollah et al., 2020), while depleted fields could offer a further 3.8 Gt of storage (APEC, 2005). However, despite the wealth of data from decades of exploration and production, there is still substantial uncertainty about how a $CO_2$ plume and its associated pressure buildup will interact with geological structure (anticlines and faults), heterogeneous reservoir distributions, and variable seal efficacies. This will ultimately lead to errors in calculating storage capacity, particularly in saline aquifers with less subsurface data available.

We aim to estimate the effective storage capacity of the J Area with limited subsurface data, but without relying on static and generalised efficiency factors. We do not include a detailed analysis of reservoir properties and instead focus on how reservoir topography and injection well location impact plume behaviour, and consequently, storage containment. By deploying a series of models within MRST co2lab (Andersen et al., 2016; Lie, 2019) we aim to answer

these questions using a physics-informed, but computationally efficient workflow that could be used more generally to assess aquifers in other basins with limited data.

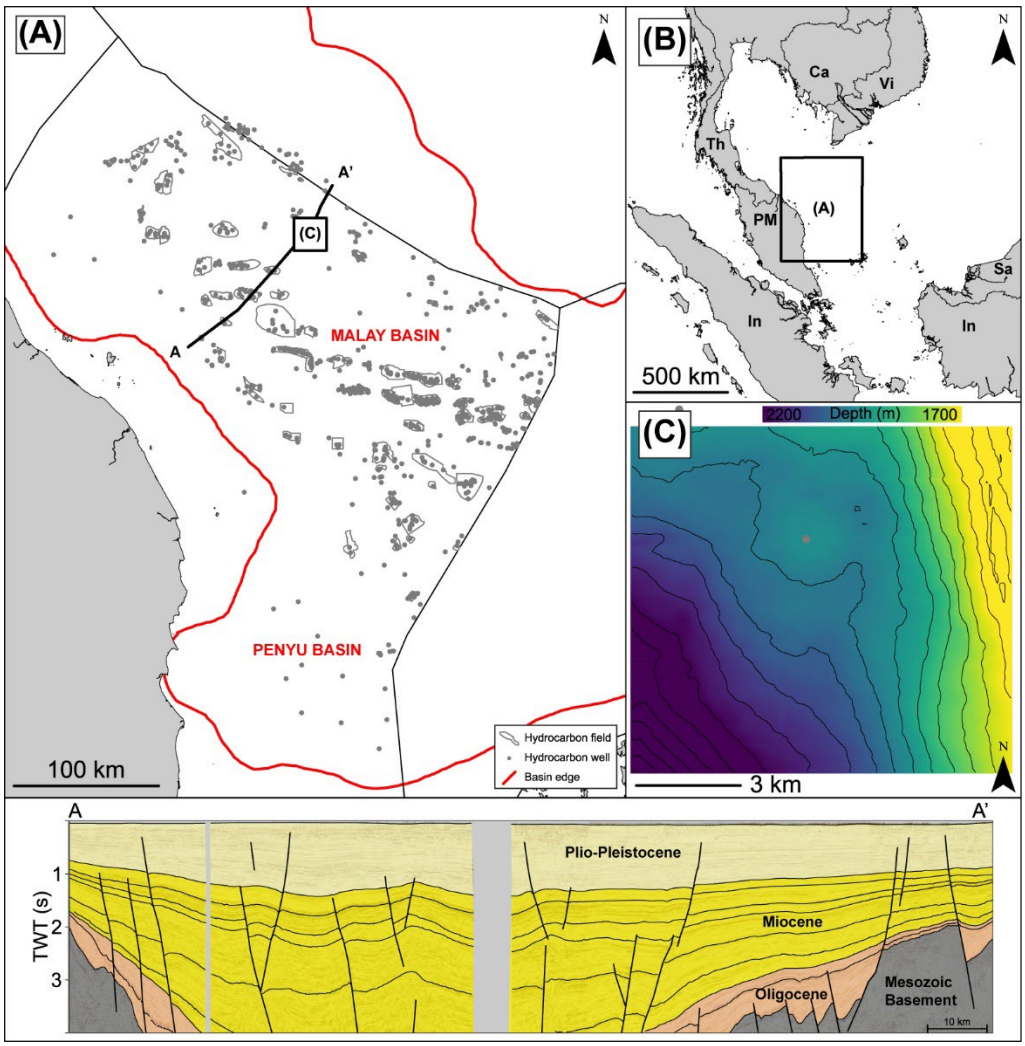


*Figure 1: (A) Map of offshore Peninsular Malaysia showing the outlines of major sedimentary basins, hydrocarbon fields, wells and the locations of (C) and cross-section A-A'. (B) Inset map showing (A)'s position in relation to the wider Southeast Asia region. (C) Top reservoir surface map in the J Area. A-A': Seismic cross-section showing the main stratigraphic units (after de Jonge-Anderson et al. (2024). Ca: Cambodia, In: Indonesia, PM: Peninsular Malaysia, Th: Thailand, TWT: two-way-time, Vi: Vietnam*

## 2. Data and Methodology

The first step in creating our geological model involved the interpretation of a time-domain 3D seismic dataset to produce a surface that is used for the structure of the grid. The surface was created within Petrel E&P software by auto-tracking a high amplitude seismic event in the J Area and gridding this at a 200 m by 200 m (X and Y) resolution. The surface was then depth-

converted using a single-layer velocity model constrained by checkshot data (de Jonge-Anderson et al., 2024). For our analysis, a simple 3D grid was constructed by duplicating this surface, shifting this duplicated surface 1000 m deeper, and then creating five equally spaced layers between. This resulted in a coarse, 200 m x 200 m x 200 m grid (Table 1). This grid was exported from Petrel E&P software in .GRDECL format and loaded into MATLAB for all subsequent analysis. Two MRST-co2lab tools were then used to determine storage capacity and efficiency.

## 2.1. Trap Analysis Functions

Trapping analysis functions originally reported by Nilsen et al. (2015) were used to map and quantify the volumes of structural traps. These functions use the geometry of the top surface to analyse the trapping framework. Structural traps, spill paths, and spill regions are determined using an algorithm previously described by Nilsen et al. (2015). Structural traps consist of a local maximum (a structural high) and a spill point (a depth contour below which $CO_2$ is expected to move up-dip and away from the local maximum), with a trap between. Structural traps are connected by spill paths that provide routes for $CO_2$ to migrate up-dip either into another trap or toward the edges of the model. Each structural trap is surrounded by a spill region; essentially a catchment area that feeds the given trap.

## 2.2. VE Model

Secondly, VE models (Nilsen et al., 2016) were used to simulate plume migration for a range of well injection locations. Trap analysis was performed in a 'static' sense whereby only the top of the reservoir (or base of the caprock) is considered, and VE modelling simulates 2D plume migration before reconstructing gas saturation for the full reservoir thickness. $CO_2$ dissolution into aqueous phase is not considered in this model.

For the VE modelling, it was also necessary to define a static petrophysical model and a simulation schedule. The gross reservoir interval consists of a heterogeneous and thick sequence of lower-middle Miocene sandstones, mudstones, and coals. During the early-middle Miocene, The J Area lay in a coastal plain-to-shoreface setting, close to sea level, with sandstone beds representing offshore sand bars, fluvial channels, or estuarine channels. While no core or cuttings data was available for this area, published data suggests sandstone reservoirs in the basin typically have porosities of between 0.1 and 0.2 (Kuttan et al., 1980).

For the petrophysical model, porosity values were assigned to each grid cell using a Gaussian field with bounds of 0.05 and 0.25 with a standard deviation of 0.02 (Figure 3). Permeability values were estimated from porosity using the Carman-Kozeny empirical relationship (Carman, 1937). There was no information available to specify irreducible water saturation, so it was fixed at 0.27, within the 0.2 – 0.4 range typical of water-wet sandstones (Baker et al., 2015).

The top reservoir lies at depths of between 1500 m and 2500 m subsea, dipping southwest (Figure 2). There is a small anticline with a crest at around 2000 m, and assuming the reservoir is at hydrostatic pressure (10 MPa/km), this is equivalent to 20 MPa. The Malay Basin is a hot basin with geothermal gradients in the J Area of around 50°C/km and a seabed temperature of 24°C (Madon & Jong, 2021), therefore a temperature of 124 °C is expected at 2000 m. Under these pressure and temperature conditions, $CO_2$ would behave as a supercritical fluid with a density of 389.70 kg/m$^3$ (Table 1).

A simulation schedule consisting of 128 timesteps was then created. This schedule consisted of 30, 1-year timesteps corresponding to the injection period, followed by 95, 10-year timesteps corresponding to the post-injection period (1000 years in total). The key metric to

assess the well placement was to ensure all the injected $CO_2$ remains within the grid/target formation. During the injection period, a single well was used to inject 1 Mt of $CO_2$ per year into the grid. Hydrostatic conditions were assigned to the boundary cells of the grid, allowing brine and $CO_2$ to flow out of the grid where necessary.

*Table 1: Model information. [1]Madon & Jong (2021); [2]Batzle & Wang (1992), [3]Fenghour et al. (1998), [4]Span & Wagner (2003)*

| Type | Property | Value |
|---|---|---|
| **Grid** | Number of cells (NX*NY*NZ) | 100 x 110 x 5 |
| | Cell dimensions (DX*DY) (m) | 200 x 200 |
| | Area ($km^2$) | 440 (22 x 20) |
| | Average top reservoir depth (m) | 1984.00 |
| | Seafloor temperature (°C)[1] | 24.00 |
| | Temperature gradient (°C/km)[1] | 50.00 |
| | Water depth (m) | 70.00 |
| **Rock** | Porosity | 0.05 – 0.25 (arithmetic mean = 0.15) |
| | Permeability (mD) | 1.20 – 241.00 (arithmetic mean = 39.40) |
| | Rock compressibility ($Pa^{-1}$) | $4.35 \times 10^{-10}$ |
| **Fluid (at 2000 m depth)** | Brine viscosity (Pa.s)[2] | $3.13 \times 10^{-4}$ |
| | Brine density ($kg/m^3$)[2] | 1001.00 |
| | Brine salinity (ppm) | 70,000 |
| | Brine compressibility ($Pa^{-1}$) | 0 |
| | $CO_2$ viscosity (Pa.s)[3] | $3.21 \times 10^{-5}$ |
| | $CO_2$ density ($kg/m^3$)[4] | 389.70 |
| | $CO_2$ compressibility ($Pa^{-1}$) | $5.78 \times 10^{-8}$ |
| **Rock-fluid** | Residual gas ($CO_2$) saturation ($s_{gr}$) | 0.20 |
| | Irreducible water saturation | 0.27 |
| | Relative permeability model | $\left(\frac{s_g - s_{gr}}{1 - s_{gr}}\right)^2$ |

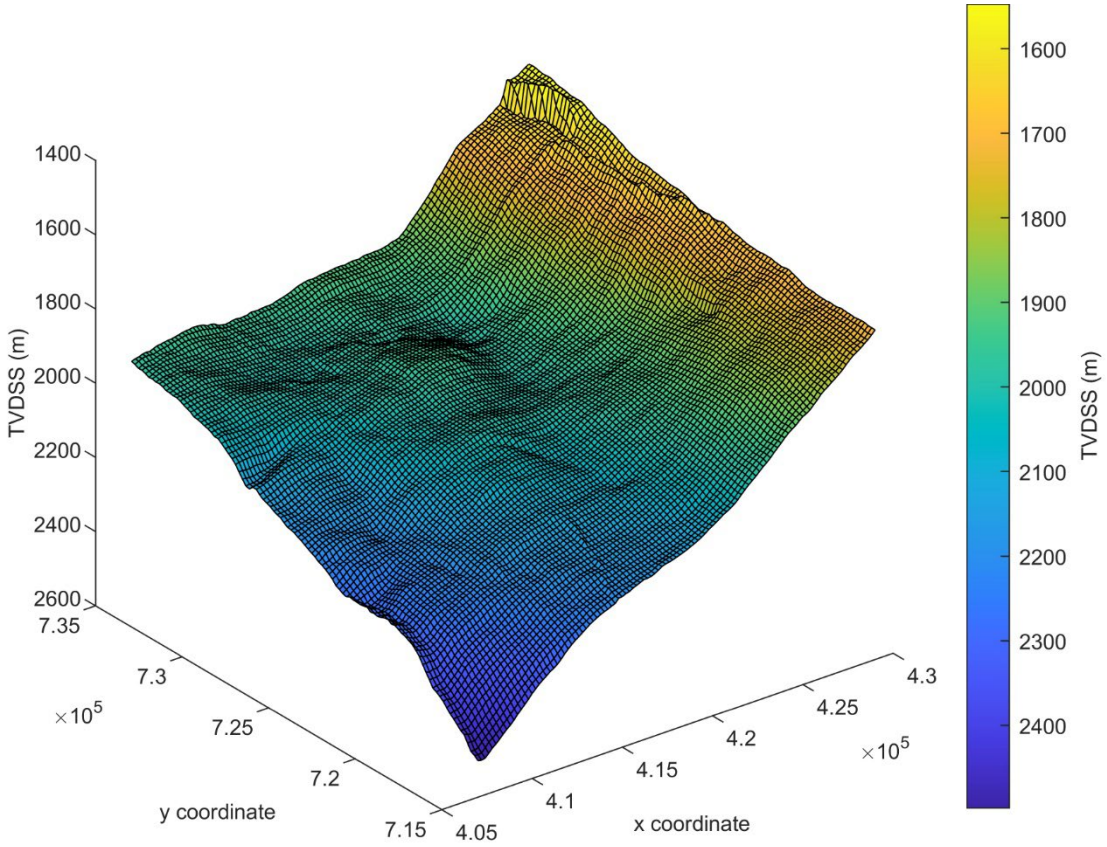


*Figure 2: The top surface grid used for trap analysis and simulations.*

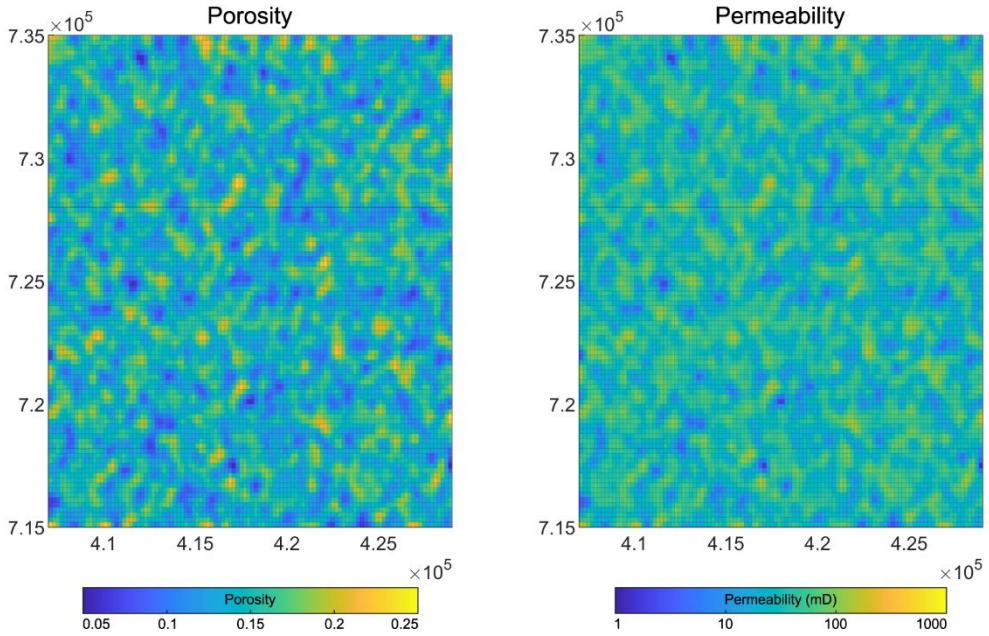


*Figure 3: Porosity (left) and permeability (right) distributions for the top reservoir surface. The porosity distribution was created by a Gaussian field with limits of between 0.05 and 0.25 and a standard deviation of 0.02. The permeability distribution was estimated from porosity using the Carman-Kozeny empirical relationship (Carman, 1937).*

# 3. Results

## 3.1. Spill point analysis

The total rock volume in our model is 440,000 $Mm^3$. However, only a subset of this volume is within structural traps where mobile $CO_2$ could accumulate. These structurally elevated areas are key in providing short-term trapping of $CO_2$ until medium-long-term processes (residual, solubility, and mineral trapping) occur. A static trapping framework for the J Area was developed **(**Figure 4) and from this, we calculated the rock volume within structural traps (along the top structure grid, only) as 202 $Mm^3$. The area dips to the southwest with an anticline in the centre (Figures 2, 4). At 195 $Mm^3$, this anticline accounts for 97 % of the entire structural trapping volume of the area. The remaining 3 % is spread mainly across four smaller traps of between 0.8 Mm3 and 3.3 $Mm^3$, with the rest held within traps down to almost negligible volumes (< 0.01 $Mm^3$).

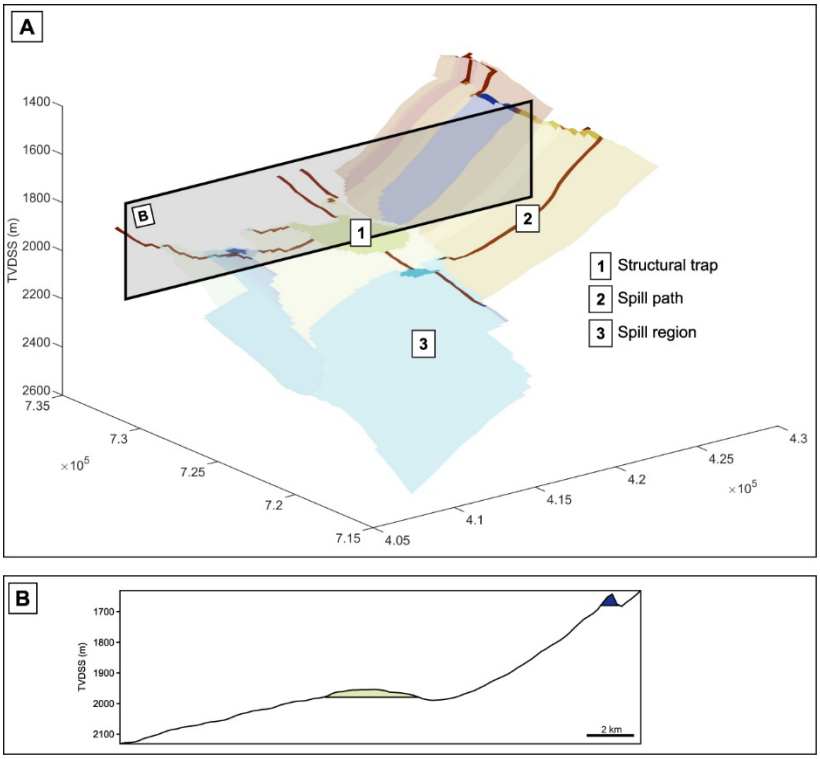


*Figure 4: A: Map of structural traps, spill paths, and spill regions identified using the 'Trap Analysis' function in MRST-co2lab, B: cross-section through the top surface grid highlighting two structural closures and the intervening, highly dipping region. The location of the line is shown in A.*

## 3.2. Trapping chains

An initial understanding of the ideal well placement is gained from analysing the trapping chains within the system. Trapping chains are essentially a series of traps that could be accessed within a "fill and spill" injection scenario. We assume infinite $CO_2$ injection such that any trap along a migration pathway can be fully filled before $CO_2$ spills and moves into the next trap (or outside of the grid). In doing this, no injection simulations are performed but a concept emerges as to how to access the maximum trapping structure within a static analysis framework (Nilsen et al., 2015). Figure 5 shows three well placements with three contrasting trapping chains. In the first example (red area in the centre of the grid), a well is placed within a small trap down-dip of the anticline. If this trap were filled to spill, $CO_2$ would migrate into, and fill, the anticline, before leaving the model to the north. This results in most of the trapping volume of the grid being accessed (197 $Mm^3$). By contrast, placing injection wells in either the downdip west (green) or updip east (blue) areas, results in $CO_2$ migration into only small structures (4.5 $Mm^3$ and 0.8 $Mm^3$, respectively).

This concept is thought of as a "reachable volume": the total trapping volume that can be accessed from a given grid cell. Figure 6 shows the grid with colouring corresponding to the reachable volume of that cell. Here, the anticline and the region downdip and to the southwest of it is the optimal well location considering purely the volume of traps accessed.

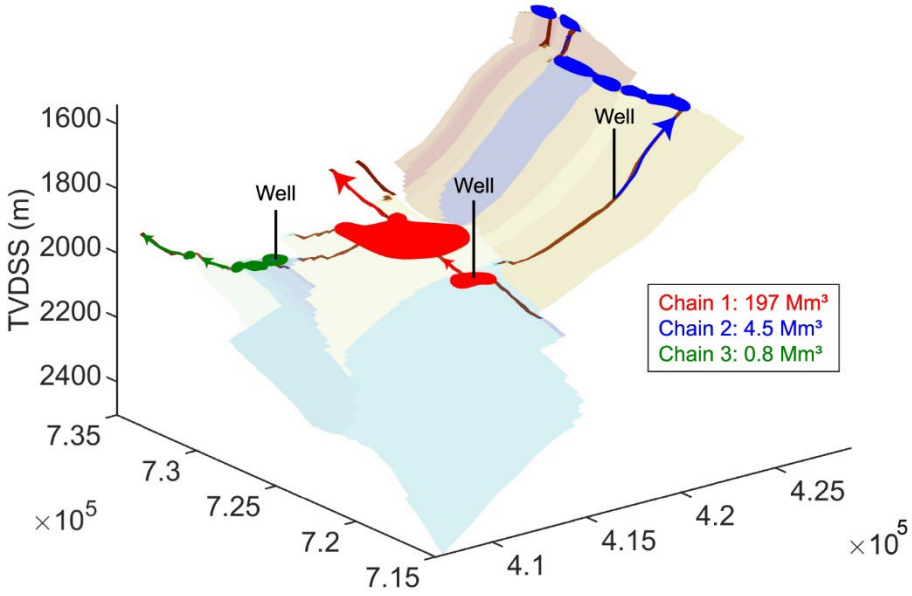


*Figure 5: Map of trapping framework (as per Figure 4) with three contrasting trapping chains and their associated trapping volumes.*

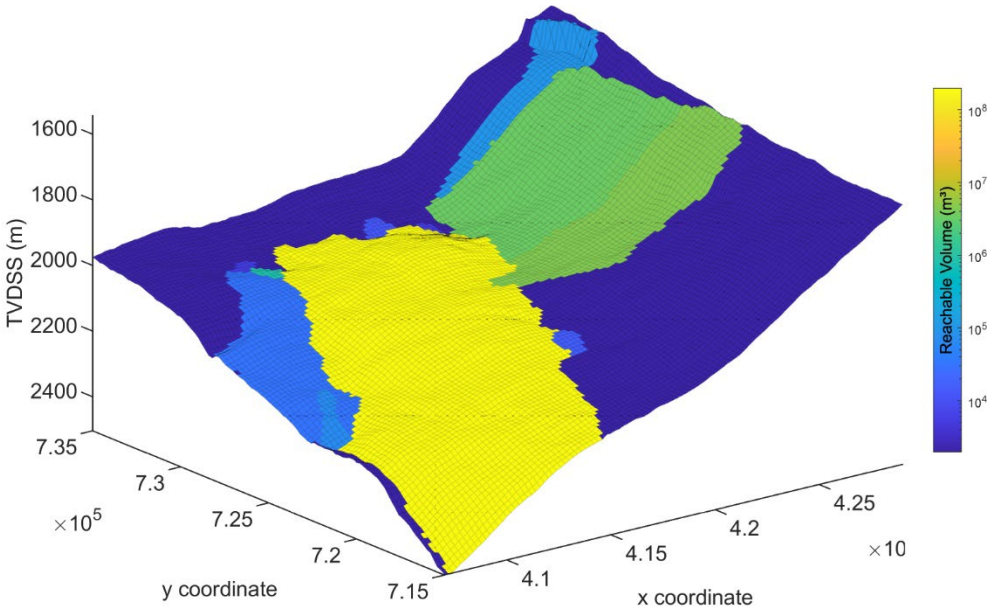


*Figure 6: Map of the top structure grid coloured by reachable volume, i.e. the volume of the grid cells within structural closures that are up-dip from that cell.*

## 3.3. Vertical equilibrium modelling

The analysis undertaken so far yields a better understanding of where to place an injector well in the area, based purely on a static analysis of the geometry of the top surface. We have not yet included the impact of the reservoir's petrophysical properties on the flow behaviour and migration of $CO_2$. To incorporate this, we use a Vertical Equilibrium (VE) model to simulate injection, as outlined in Section 2.2. This requires static petrophysical models of porosity and

permeability (Figure 3). Taking this model into account, the area's total pore volume is 63,794 $Mm^3$, which can store approximately 25 Gt of $CO_2$, assuming the $CO_2$ density listed in Table 1.

The computational efficiency of VE models allows us to run different iterations and test various uncertainties very quickly. For this study, we concentrate only on determining the optimal location for an injection well. The injection location has a significant influence on $CO_2$ plume migration and containment of $CO_2$ within the area. To assess this, a systematic analysis was undertaken to constrain the best injection well location on the grid. For this, we assumed the best well location is where the highest storage efficiency is achieved. We first calculate the $CO_2$ volume $v_{CO2}$ remaining within the grid at the end of the migration period and divide this by the total pore volume of the grid $v_P$. The storage efficiency ε is defined as

$$\varepsilon = \frac{v_{CO2}}{v_p} \times 100.$$

A simulation was performed with an injection well at every $25^{th}$ grid cell, resulting in 440 simulations across the 11,000-cell top surface grid. Each iteration ran in around 45 seconds on an Intel Xeon Gold 6240R 2.4 GHz CPU. Our objective was to determine which of these 440 injection locations minimised leakage away from the model boundary (a proxy for a storage licence) and in doing so, maximised the amount of $CO_2$ being stored within the area, and the storage efficiency ε. The total trapped $CO_2$ volume and storage efficiency were mapped from the results of all the simulations (Figure 7B, C). The amount of $CO_2$ stored within the model at the end of the simulation period was variable, ranging from 0.77 $Mm^3$ to 101.27 $Mm^3$ (Table 2). The corresponding storage efficiencies ranged from 0.0017 % to 0.22 % (Figure 7C).

The lowest storage efficiencies and trapped $CO_2$ volumes were near the model boundaries where most injected $CO_2$ exited the model (Figure 7C). The highest storage efficiencies and trapped $CO_2$ volumes were observed when the well was positioned in the lower-left side of

the model (Figure 7C). In these cases, there was not only a sizeable area of up-dip, unconfined reservoir available for the $CO_2$ to migrate to but also an anticline which would eventually form a trap for the migrating $CO_2$ plume (Figure 7D). Notably, injection directly into this anticline itself resulted in lower storage efficiencies and stored volumes, as the anticline was quickly filled-to-spill and the $CO_2$ then migrated northwards and out of the model. From this analysis, we can conclude that the optimal well location was at the coordinate pair (410100 m, 721700 m) (Figure 7D), with a storage efficiency of 0.22 % and a capacity of 101.27 $Mm^3$. (Table 2).

*Table 2. Summary of $CO_2$ capacities determined at each stage of our analysis. *Structural trapping is only calculated for the top surface of the grid, so it is significantly smaller than other volume metrics*

| Calculation type | Capacity Description | Capacity (Mm3) |
|---|---|---|
| Entire grid | Total rock volume | 440,000 |
| | Total pore volume | 63,794 |
| Structural trapping (along top surface*) | Total pore volume within structural traps | 29 |
| VE model | Trapped $CO_2$ volume (max) | 101.27 |
| | Trapped $CO_2$ volume (min) | 0.77 |

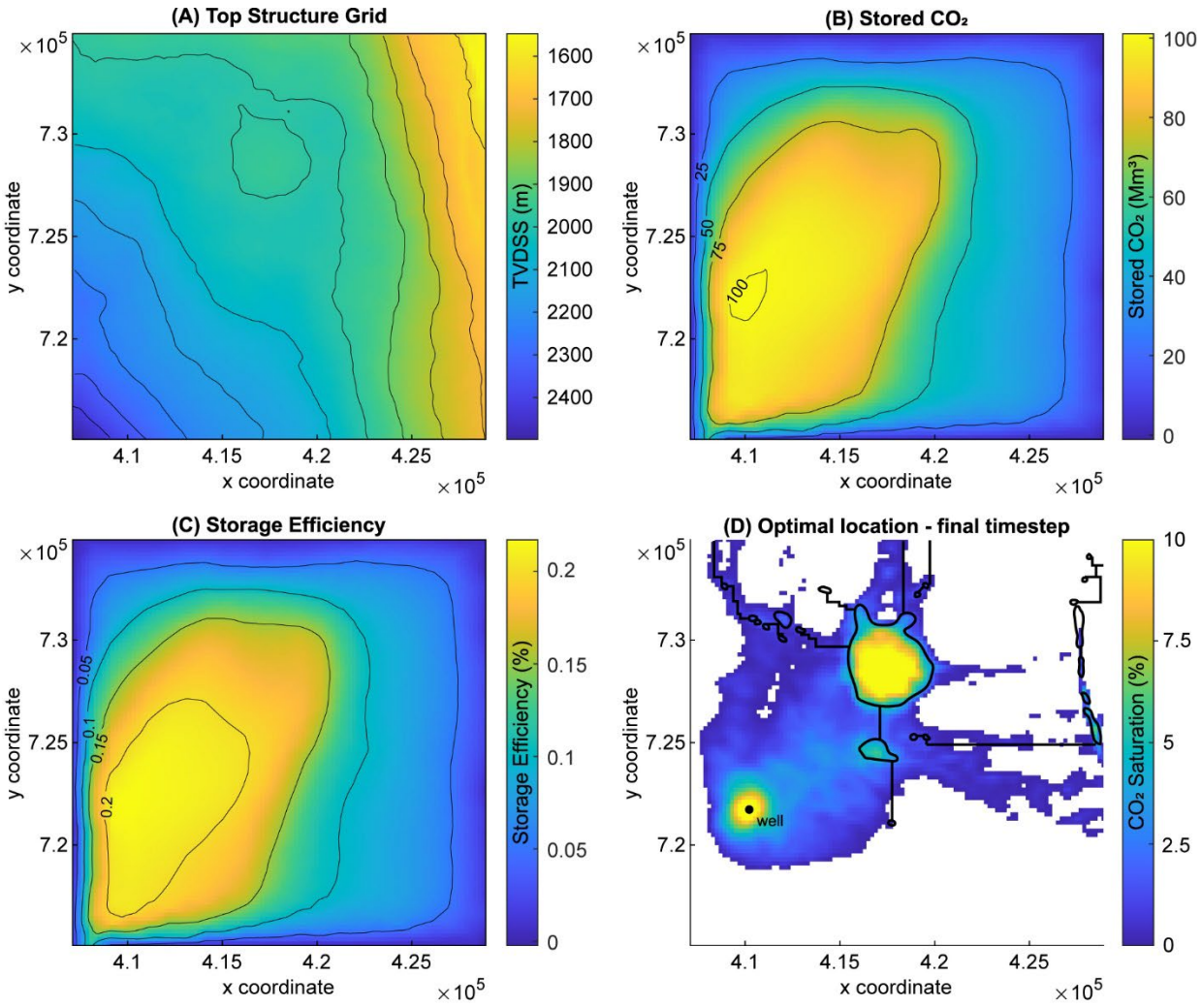


*Figure 7: Output maps from the VE modelling showing (A) the top structure of the reservoir, (B) stored $CO_2$ volume, (C) storage efficiency and (D) the final saturation distribution of $CO_2$ for the optimal well location.*

## 4. Discussion

When screening $CO_2$ storage sites, efficiency is often handled either through a series of coefficients or using analytical solutions. Certain studies propose storage coefficients or classifications of storage efficiency based on numerical simulations or laboratory work, that are extrapolated to other aquifers based on shared characteristics (often the depositional environment, lithology, or petrophysical behaviour) (e.g., Gorecki et al., 2009; Blondes et al., 2013; Brennan, 2014). Analytical solutions can offer quick solutions but often assume that the reservoir is homogeneous and/or the aquifer is closed (Okwen et al.,2010; Szulczewski et al., 2012; Zhou et al., 2008). Storage efficiency is ultimately a dynamic property that evolves with

injection time (Okwen et al., 2014; Szulczewski et al., 2014). Bachu (2015) suggested that volumetric approaches to storage efficiency were adequate at the screening level, but these should be replaced at the local level by numerical simulations incorporating various operational and regulatory constraints. To this effect, there has been much recent research into developing fast tools for CCS screening utilising VE modelling (Lie et al., 2016), sketch-based modelling (Jackson et al., 2022; Petrovskyy et al., 2023) or reduced-order models (Jin & Durlofsky, 2018). In this work, we utilise VE models to enable numerical modelling at the screening stage, to quickly simulate uncertain parameters and estimate the dynamic plume behaviour, which is lacking in volumetric approaches to capacity/efficiency estimation.

Using a conservative storage efficiency factor of 2.4% (Goodman et al., 2011) and the area properties mentioned in Table 1, one can calculate the J Area's static capacity as 1531.06 $Mm^3$. However, the results from VE modelling indicate that the amount that can be contained within the area is 15 times less, at 101.27 $Mm^3$ (Table 2). This result clearly shows the importance of dynamic effects and their constraint on storage capacity. Accounting for these effects is essential to avoid overestimating storage capacity, especially at the site screening phase.

The strength of our approach is the speed at which the static and dynamic tools described herein can be used to predict reliable storage capacity with limited data. A simulation takes less than one minute to run for this particular storage site, so an exercise to find the optimal well location that maximises storage efficiency is executed in a few hours While fully-coupled 3D simulations are accurate, they would require weeks of simulation time to address the same problem. Hence, this approach is useful in addressing uncertainty and its impact on storage efficiency. There are certain limitations to our current work that could be addressed through follow-up studies. Many of these limitations pertain to the construction of the geological

model. Our work treats the reservoir as a vertically homogenous unit with porosity and permeability characteristics typical of average values in the Malay Basin, but these reservoirs are very layered, with many, thin reservoir intervals separated by low-permeability mudstones. A more accurate representation of this could be achieved by reducing the reservoir thickness to an appropriate value and/or incorporating a layered reservoir-seal system using hybrid-VE modelling (Møyner & Nilsen, 2019). There is scope to develop sophisticated petrophysical models that reflect the depositional characteristics of the reservoir, particularly as such features can be imaged using seismic attributes in the Malay Basin (Ghosh et al., 2010).

The maximum storage efficiency modelled is low, at 0.22 %, but it is important to emphasise that this value because we considered only structural and residual trapping. The fluid compressibility, gas solubility and geochemistry were not considered. Also, this is a single-well injection scenario with an open model boundary without any consideration for pressure management. Accounting for these factors would increase the storage efficiency and capacity prediction. Further work could focus on understanding the pressure buildup and its influence on geomechanical properties within the reservoir and caprock as the magnitude and extent of pressure perturbation may also constrain the storage capacity of the system (Bachu, 2015; Birkholzer et al., 2015). Given the topographical variations across the top surface grid, it would be sensible to monitor reservoir pressure in the far up-dip area in the northeast to ensure these are not approaching or exceeding fracture pressures.

## 5. Conclusions

A workflow for assessing the storage capacity and efficiency of a saline aquifer is presented, through combining static and dynamic reduced complexity tools. These tools include static

methods (automated identification of structural traps and optimization of well location to access the greatest trapping volume) and dynamic methods (VE models). In the case of the latter, the greatly reduced computational running time allows us to run optimization procedures and sensitivity analysis around uncertain parameters; an approach that cannot be undertaken with more powerful, but computationally expensive reservoir simulators. We apply these techniques to an area offshore Malaysia with illustrative reservoir parameters and focus strictly on $CO_2$ plume migration obtained from VE modelling. The main conclusions taken from this work are as follows:

(1) Taking a volumetric approach to storage capacity results in unrealistically large values. The key finding is that the storage capacity derived from VE modelling is two orders of magnitude smaller than that derived from the total pore volume for the area.

(2) The upper bound on storage efficiency is ultimately dictated by how much $CO_2$ is injected into the aquifer system without suffering leakage away from the model boundary (a proxy for a storage licence). We analysed well placement by performing hundreds of simulations and calculating storage efficiency. This resulted in the best location for our area being down-dip of an anticline structure into which the $CO_2$ would migrate during the post-injection period.

(3) There is general agreement between static and dynamic approaches to well placement optimization. The area with the greatest “reachable volume” corresponds to the area highlighted by VE modelling as achieving the greatest storage efficiency, though this result could change with different porosity/permeability distributions. However, storage capacities defined by static models are still theoretical maximums and simulations should be used to assess to what extent pore space can be accessed, incorporating physics and spatial changes in geology.

# References


Andersen, O., Lie, K.-A., & Nilsen, H. M. (2016). An open-source toolchain for simulation and optimization of aquifer-wide co2 storage. Energy Procedia, 86, 324–333. https://doi.org/10.1016/j.egypro.2016.01.033

APEC. (2005). CO2 Storage Prospectivity of Selected Sedimentary Basins in the Region of China and South East Asia, June 2005. https://www.apec.org/Publications/2005/06/CO2-Storage-Prospectivity-of-Selected-Sedimentary-Basins-in-the-Region-of-China-and-South-East-Asia

Bachu, S. (2015). Review of CO2 storage efficiency in deep saline aquifers. International Journal of Greenhouse Gas Control, 40, 188–202. https://doi.org/10.1016/j.ijggc.2015.01.007

Bachu, S., Bonijoly, D., Bradshaw, J., Burruss, R., Holloway, S., Christensen, N. P., & Mathiassen, O. M. (2007). CO2 storage capacity estimation: Methodology and gaps. International Journal of Greenhouse Gas Control, 1(4), 430–443. https://doi.org/10.1016/S1750-5836(07)00086-2

Baker, R. O., Yarranton, H. W., & Jensen, J. L. (2015). Special core analysis—Rock–fluid interactions. In Practical Reservoir Engineering and Characterization (pp. 239–295). Elsevier. https://doi.org/10.1016/B978-0-12-801811-8.00008-0

Batzle, M., & Wang, Z. (1992). Seismic properties of pore fluids. GEOPHYSICS, 57(11), 1396–1408. https://doi.org/10.1190/1.1443207

Bentham, M., Mallows, T., Lowndes, J., & Green, A. (2014). CO2 storage evaluation database (Co2 stored). The UK's online storage atlas. Energy Procedia, 63, 5103–5113. https://doi.org/10.1016/j.egypro.2014.11.540

Birkholzer, J. T., Oldenburg, C. M., & Zhou, Q. (2015). CO2 migration and pressure evolution in deep saline aquifers. International Journal of Greenhouse Gas Control, 40, 203–220. https://doi.org/10.1016/j.ijggc.2015.03.022

Blondes, M.S., Brennan, S.T., Merrill, M.D., Buursink, M.L., Warwick, P.D., Cahan, S.M., Cook, T.A., Corum, M.D., Craddock, W.H., DeVera, C.A, Drake, R.M., II, Drew, L.J., Freeman, P.A., Lohr, C.D., Olea, R.A., Roberts-Ashby, T.L., Slucher, E.R., and Varela, B.A. (2013). National assessment of geologic carbon dioxide storage resources—Methodology implementation: U.S. Geological Survey Open-File Report 2013–1055, 26 p., http://pubs.usgs.gov/of/2013/1055/.

Brennan, S. T. (2014). The U. S. Geological Survey carbon dioxide storage efficiency value methodology: Results and observations. Energy Procedia, 63, 5123–5129. https://doi.org/10.1016/j.egypro.2014.11.542

Carman, C. P. (1937). Fluid flow through a granular bed. Trans. Inst. Chem. Eng. London, 15, 150–156. https://cir.nii.ac.jp/crid/1571698600457019392

de Jonge-Anderson, I., Widyanita, A., Busch, A., Doster, F., & Nicholson, U. (2024). New insights into the structural and stratigraphic evolution of the Malay basin using 3d seismic data:

366 Implications for regional carbon capture and storage potential [Preprint]. Physical
367 Sciences and Mathematics. https://doi.org/10.31223/X5MQ20

368 Fenghour, A., Wakeham, W. A., & Vesovic, V. (1998). The viscosity of carbon dioxide. Journal
369 of Physical and Chemical Reference Data, 27(1), 31–44.
370 https://doi.org/10.1063/1.556013

371 Gasda, S. E., Nordbotten, J. M., & Celia, M. A. (2009). Vertical equilibrium with sub-scale
372 analytical methods for geological CO2 sequestration. Computational Geosciences,
373 13(4), 469–481. https://doi.org/10.1007/s10596-009-9138-x

374 Ghosh, D. P., Ibrahim, N. A., Viratno, B., & Mohamad, H. (2010). Seismic attributes adding a
375 new dimension to prospect evaluation & geomorphology identification in the malay
376 and adjacent basins. SEG Technical Program Expanded Abstracts 2010, 1307–1311.
377 https://doi.org/10.1190/1.3513083

378 Goodman, A., Hakala, A., Bromhal, G., Deel, D., Rodosta, T., Frailey, S., Small, M., Allen, D.,
379 Romanov, V., Fazio, J., Huerta, N., McIntyre, D., Kutchko, B., & Guthrie, G. (2011). U.S.
380 DOE methodology for the development of geologic storage potential for carbon
381 dioxide at the national and regional scale. International Journal of Greenhouse Gas
382 Control, 5(4), 952–965. https://doi.org/10.1016/j.ijggc.2011.03.010

383 Gorecki, C. D., Sorensen, J. A., Bremer, J. M., Knudsen, D. J., Smith, S. A., Steadman, E. N., &
384 Harju, J. A. (2009). Development of storage coefficients for determining the effective
385 co2 storage resource in deep saline formations. All Days, SPE-126444-MS.
386 https://doi.org/10.2118/126444-MS

387 Hasbollah, D. Z. A., Junin, R., Taib, A. M., & Mazlan, A. N. (2020). Basin evaluation of co2
388 geological storage potential in malay basin, malaysia. In P. Duc Long & N. T. Dung (Eds.),
389 Geotechnics for Sustainable Infrastructure Development (Vol. 62, pp. 1405–1410).
390 Springer Singapore. https://doi.org/10.1007/978-981-15-2184-3_184

391 IPCC. (2023). Climate Change 2023: Synthesis Report. Contribution of Working Groups I, II and
392 III to the Sixth Assessment Report of the Intergovernmental Panel on Climate Change
393 [Core Writing Team, H. Lee and J. Romero (eds.)]. IPCC, Geneva, Switzerland, 184 pp.,
394 https://doi.org/10.59327/IPCC/AR6-9789291691647

395 Jackson, W. A., Hampson, G. J., Jacquemyn, C., Jackson, M. D., Petrovskyy, D., Geiger, S.,
396 Machado Silva, J. D., Judice, S., Rahman, F., & Costa Sousa, M. (2022). A screening
397 assessment of the impact of sedimentological heterogeneity on CO2 migration and
398 stratigraphic-baffling potential: Johansen and Cook formations, Northern Lights
399 project, offshore Norway. International Journal of Greenhouse Gas Control, 120,
400 103762. https://doi.org/10.1016/j.ijggc.2022.103762

401 Jin, Z. L., & Durlofsky, L. J. (2018). Reduced-order modeling of CO2 storage operations.
402 International Journal of Greenhouse Gas Control, 68, 49–67.
403 https://doi.org/10.1016/j.ijggc.2017.08.017

404 Kuttan, K., Stockbridge, C. P., Crocker, H., & Remfry, J. G. (1980). Log interpretation in the malay
405 basin. SPWLA 21st Annual Logging Symposium

Lie, K.-A. (2019). An introduction to reservoir simulation using matlab/gnu octave: User guide for the matlab reservoir simulation toolbox (Mrst) (1st ed.). Cambridge University Press. https://doi.org/10.1017/9781108591416

Madon, M., & Jong, J. (2021). Geothermal gradient and heat flow maps of offshore malaysia: Some updates and observations. Bulletin of the Geological Society of Malaysia, 71, 159–183. https://doi.org/10.7186/bgsm71202114

Mathias, S. A., Gluyas, J. G., Goldthorpe, W. H., & Mackay, E. J. (2015). Impact of maximum allowable cost on co 2 storage capacity in saline formations. Environmental Science & Technology, 49(22), 13510–13518. https://doi.org/10.1021/acs.est.5b02836

Møyner, O., & Nilsen, H. M. (2019). Multiresolution coupled vertical equilibrium model for fast flexible simulation of CO2 storage. Computational Geosciences, 23(1), 1–20. https://doi.org/10.1007/s10596-018-9775-z

Nilsen, H. M., Herrera, P. A., Ashraf, M., Ligaarden, I., Iding, M., Hermanrud, C., Lie, K.-A., Nordbotten, J. M., Dahle, H. K., & Keilegavlen, E. (2011). Field-case simulation of CO2 -plume migration using vertical-equilibrium models. Energy Procedia, 4, 3801–3808. https://doi.org/10.1016/j.egypro.2011.02.315

Nilsen, H. M., Lie, K.-A., Møyner, O., & Andersen, O. (2015). Spill-point analysis and structural trapping capacity in saline aquifers using MRST-co2lab. Computers & Geosciences, 75, 33–43. https://doi.org/10.1016/j.cageo.2014.11.002

Nilsen, H. M., Lie, K.-A., & Andersen, O. (2016). Robust simulation of sharp-interface models for fast estimation of CO2 trapping capacity in large-scale aquifer systems. Computational Geosciences, 20(1), 93–113. https://doi.org/10.1007/s10596-015-9549-9

Nordbotten, J. M., Celia, M. A., & Bachu, S. (2005). Injection and storage of co2 in deep saline aquifers: Analytical solution for co2 plume evolution during injection. Transport in Porous Media, 58(3), 339–360. https://doi.org/10.1007/s11242-004-0670-9

Nordbotten, J. M., & Celia, M. A. (2011). Geological storage of co2: Modeling approaches for large-scale simulation (1st ed.). Wiley. https://doi.org/10.1002/9781118137086

Okwen, R. T., Stewart, M. T., & Cunningham, J. A. (2010). Analytical solution for estimating storage efficiency of geologic sequestration of CO2. International Journal of Greenhouse Gas Control, 4(1), 102–107. https://doi.org/10.1016/j.ijggc.2009.11.002

Okwen, R., Yang, F., & Frailey, S. (2014). Effect of geologic depositional environment on co2 storage efficiency. Energy Procedia, 63, 5247–5257. https://doi.org/10.1016/j.egypro.2014.11.556

Petrovskyy, D., Jacquemyn, C., Geiger, S., Jackson, M. D., Hampson, G. J., Machado Silva, J. D., Judice, S., Rahman, F., & Costa Sousa, M. (2023). Rapid flow diagnostics for prototyping of reservoir concepts and models for subsurface CO2 storage. International Journal of Greenhouse Gas Control, 124, 103855. https://doi.org/10.1016/j.ijggc.2023.103855

Span, R., & Wagner, W. (2003). Equations of State for Technical Applications. I. Simultaneously Optimized Functional Forms for Nonpolar and Polar Fluids. International Journal of Thermophysics, 24(1), 1–39. https://doi.org/10.1023/A:1022390430888

Szulczewski, M. L., MacMinn, C. W., Herzog, H. J., & Juanes, R. (2012). Lifetime of carbon capture and storage as a climate-change mitigation technology. Proceedings of the National Academy of Sciences, 109(14), 5185–5189. https://doi.org/10.1073/pnas.1115347109

Szulczewski, M. L., MacMinn, C. W., & Juanes, R. (2014). Theoretical analysis of how pressure buildup and CO2 migration can both constrain storage capacity in deep saline aquifers. International Journal of Greenhouse Gas Control, 23, 113–118. https://doi.org/10.1016/j.ijggc.2014.02.006

The MATLAB Reservoir Simulation Toolbox, version 2023b, https://www.sintef.no/projectweb/mrst/ (January 2024)

The MATLAB Reservoir Simulation Toolbox: Numerical CO2 Laboratory, https://www.sintef.no/projectweb/mrst/modules/co2lab/ (January 2024)

Thibeau, S., & Mucha, V. (2011). Have we overestimated saline aquifer co 2 storage capacities? Oil & Gas Science and Technology – Revue d'IFP Energies Nouvelles, 66(1), 81–92. https://doi.org/10.2516/ogst/2011004

Vangkilde-Pedersen, T., Anthonsen, K. L., Smith, N., Kirk, K., Neele, F., Van Der Meer, B., Le Gallo, Y., Bossie-Codreanu, D., Wojcicki, A., Le Nindre, Y.-M., Hendriks, C., Dalhoff, F., & Peter Christensen, N. (2009). Assessing European capacity for geological storage of carbon dioxide–the EU GeoCapacity project. Energy Procedia, 1(1), 2663–2670. https://doi.org/10.1016/j.egypro.2009.02.034

Zhou, Q., Birkholzer, J. T., Tsang, C.-F., & Rutqvist, J. (2008). A method for quick assessment of CO2 storage capacity in closed and semi-closed saline formations. International Journal of Greenhouse Gas Control, 2(4), 626–639. https://doi.org/10.1016/j.ijggc.2008.02.004